ACS APPLIED MATERIALS & INTERFACES

Research Article

www.acsami.org

# Atomic-Layer-Deposition Functionalized Carbonized Mesoporous Wood Fiber for High Sulfur Loading Lithium Sulfur Batteries

Chao Luo,[†] Hongli Zhu,[‡,§] Wei Luo,[‡] Fei Shen,[‡] Xiulin Fan,[†] Jiaqi Dai,[‡] Yujia Liang,[†] Chunsheng Wang,*[,†] and Liangbing Hu*[,‡]

[†]Department of Chemical and Biomolecular Engineering and [‡]Material Science and Engineering, University of Maryland, College Park, Maryland 20742, United States

[§]Northeastern University, Department of Mechanical and Industrial Engineering, 360 Huntington Avenue, Boston, Massachusetts 02115-5005, United States

Supporting Information

**ABSTRACT:** Lithium−sulfur battery (LSB) as one of the most promising energy storage devices suffers from poor conductivity of sulfur and fast capacity decay triggered by the dissolution of polysulfides. In this work, functionalized carbonized mesoporous wood fiber (f-CMWF) is employed as a host to accommodate sulfur for the first time. Natural wood microfiber has unique hierarchical and mesoporous structure, which is well-maintained after carbonization. With such a hierarchical mesoporous structure, a high sulfur loading of 76 wt % is achieved in CMWF electrodes. The pore size of CMWF is tunable by atomic layer deposition (ALD) of a 5 nm $Al_2O_3$ coating to form the f-CMWF. Such a thin layer slightly decreases the sulfur loading to 70%, but it remarkably promotes the cyclic stability of sulfur cathode, which delivers an initial capacity of 1115 mAh $g^{-1}$, and maintains a reversible capacity of 859 mAh $g^{-1}$ for 450 cycles, corresponding to a slow capacity decay rate of 0.046% per cycle. More importantly, natural wood microfiber is first used as a raw material for sulfur encapsulating. This work is also critical for using low cost and mesoporous biomass carbon as bifunctional scaffold for LSB.

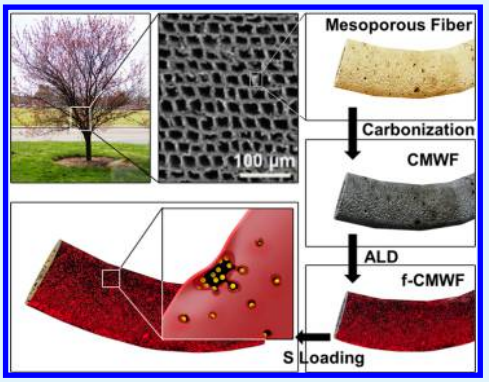


**KEYWORDS:** *lithium−sulfur battery, tunable pore size, small sulfur molecule, carbonized wood fiber, atomic layer deposition*

## INTRODUCTION

The ever-increasing demand for high-energy rechargeable batteries has driven the battery community to develop new electrode materials with higher specific capacity than the traditional intercalation-based ones, such as $LiCoO_2$ and $LiFePO_4$. Due to the low cost, large availability, environmental benignity, and high energy density of sulfur cathode, lithium−sulfur batteries (LSBs) have received considerable research interest.[1−6] The theoretical capacity of sulfur cathode is 1672 mAh $g^{-1}$, corresponding to a high energy density of 2600 Wh $kg^{-1}$, which is 3−5 times higher than the conventional intercalation-based cathodes.[7−9] Though the LSB is considered one of the most promising rechargeable batteries, there are still three intrinsic challenges which significantly impede its large-scale application: (1) The dissolution of polysulfide intermediates during charge/discharge results in low Coulombic efficiency and rapid capacity decay. (2) Low utilization of sulfur induced by the extremely low conductivity of S and $Li_2S$ reduces the capacity and power density. (3) The stress/strain caused by the significant volume change of 76% between sulfur (2.03 g $cm^{-3}$) and $Li_2S$ (1.66 g $cm^{-3}$) destroys the electrode integrity.[10−19]

In the past decade, significant progress has been made to overcome these three challenges. In 2009, Nazar's group reported that mesoporous carbon encapsulated sulfur cathode showed superior electrochemical performance, where the carbon matrix improved the conductivity of sulfur cathode and a polymer layer coating effectively trapped the polysulfide intermediates.[20] Inspired by this, a large number of carbonaceous materials including porous carbon, carbon nanotube (CNT), graphene, graphene oxide (GO), and carbon nanofiber have been investigated to further improve the performance of sulfur/carbon composites.[21−30] However, good performance of LSB is normally expected at low sulfur loading (30−60 wt %), resulting in a low overall capacity.[31] When sulfur loading is higher than 70 wt %, it is very difficult to retain the high cycling stability. Therefore, stable and high sulfur loading sulfur/carbon cathode is heavily desired for LSB.

Natural wood microfiber, an inexpensive, abundant, renewable and environmentally benign natural resource, is an ideal precursor for porous carbon. More interestingly, the naturally hierarchical and mesoporous structure in wood microfiber can be well-maintained after carbonization, which is an excellent candidate to confine the polysulfides during electrochemical

Received: January 24, 2017
Accepted: April 14, 2017
Published: April 14, 2017




DOI: 10.1021/acsami.7b01205
ACS Appl. Mater. Interfaces 2017, 9, 14801−14807

reactions. As shown in Figure 1a,b, the wood microfibers in the trees have numerous multichannels to allow the transport of

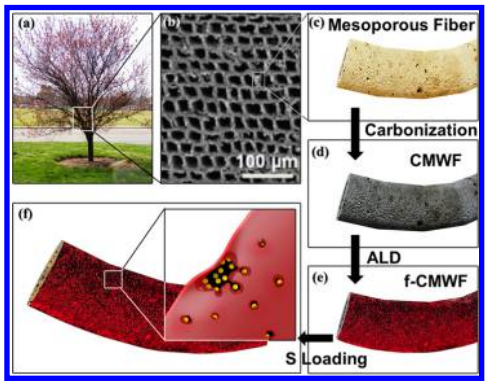


**Figure 1.** Schematic of the hierarchical and mesoporous structure of natural wood fiber. $Al_2O_3$ (5 nm) is deposited at the interface between carbon and sulfur. The small molecular sulfur is encapsulated within the carbon mesopores. (a) Picture of tree. (b) Cross-sectional SEM image of wood trunk. (c) Schematic of a single wood fiber. The gray color indicates the mesopores along the fiber. (d) Schematic of the CMWF after carbonization. The CMWF provide excellent electron transfer paths in the sulfur lithium battery. (e) Schematic of the f-CMWF with ALD $Al_2O_3$. The red color indicates $Al_2O_3$. (f) Schematic of sulfur infiltration in the $Al_2O_3$ coated f-CMWF. The yellow spheres represent sulfur.

nutrients such as water, ions, and small molecules in the tree for metabolism. Each wood microfiber consists of mesoporous channels (Figure 1b) to facilitate the transport of nutrients. The high porosity enables the wood microfiber to be a promising host for sulfur. However, since natural wood microfiber is insulating, a thin layer of conductive material, such as carbon nanotubes, has to be deposited on the fiber to act as electron transfer medium.[32−34] To endow the fiber with excellent electrical conductivity and meanwhile maintain the unique mesoporous structure, high-temperature carbonization is used to carbonize the natural wood fiber (Figure 1c) to mesoporous carbon fiber (Figure 1d) in this work. The mesoporous and multichannel structure of wood microfiber has been demonstrated to have excellent performance in supercapacitor, sodium-ion batteries, and microbial fuel cell.[35−39] However, it has not been explored as a host for sulfur cathodes.

Taking advantage of electrode manufacturing, a free-standing carbon film is fabricated from wood microfiber electrode by high-temperature treatment. Then, a thin layer (5 nm) of $Al_2O_3$ is coated on CMWF to form a functionalized CMWF (f-CMWF), as shown in Figure 1e. There are three major advantages of ALD $Al_2O_3$ for stabilizing sulfur in the CMWF: (1) $Al_2O_3$ is a very stable substrate in the free-standing sulfur electrode since it cannot react with either CMWF or sulfur. (2) The thickness of $Al_2O_3$ layer is controllable in the nanoscale by ALD. (3) The synthesis of $Al_2O_3$ by ALD is through gas-phase reaction on the surface of carbonized mesoporous wood fiber, so the reaction precursor gas can migrate into the small pores of the carbonized mesoporous wood fiber to generate $Al_2O_3$ layer inside the pore and reduce the pore size and volume in the carbonized mesoporous wood fiber. Sulfur is infused into the f-CMWF by a sealed vacuum glass tube technique, giving a sulfur/carbon cathode.[40,41] The obtained f-CMWF with smaller pore size to entrap small sulfur molecules, maintains the unique hierarchical and mesoporous structure of wood microfiber, and can accommodate up to 70 wt % sulfur, which is among the highest mass loading in the reported work.[42] The S/f-CMWF cathode (Figure 1f) displays an initial capacity of 1115 mAh $g^{-1}$ at 400 mA $g^{-1}$, and maintains a reversible capacity of 859 mAh $g^{-1}$ for 450 cycles, corresponding to a very slow capacity decay rate of 0.046% per cycle. In addition to the high sulfur loading, the free-standing S/f-CMWF cathode is a current collector-free, binder and conductive additive-free electrode, which contains negligible electrochemical inactive component. It is noteworthy that it is very difficult to achieve high long-term cyclic stability in lithium sulfur batteries when sulfur-loading is close to or above 70 wt %. In recent work, Ye et al. reported a multiwall carbon nanotube porous microspheres encapsulated sulfur cathode with 70 wt % sulfur loading, and good cyclic stability can be maintained for 100 cycles.[43] Jin et al. loaded 85.2 wt % sulfur in carbon nanotubes with a good cyclic stability for 150 cycles.[44] Fang et al. fabricated a cable-shaped lithium sulfur battery with 68 wt % sulfur loading, which shows stable cycle life for 200 cycles.[45] In our work, the free-standing S/f-CMWF cathode can deliver a reversible capacity of 859 mAh $g^{-1}$ for 450 cycles, representing one of the best sulfur cathodes with high sulfur loading (>70 wt %) to date. More importantly, natural wood microfiber is first used as a raw material for sulfur encapsulating. This work is also critical for using low-cost and mesoporous biomass carbon as bifunctional scaffold for lithium sulfur batteries.

## RESULTS AND DISCUSSION

To confirm that the unique hierarchical and mesoporous structure of wood microfiber is well-maintained after carbonization, scanning electron microscopy (SEM), transmission electron microscopy (TEM), and Brunauer−Emmett−Teller (BET) characterizations are performed to check the structure and porosity of CMWF derived from trees. Figure 2a shows a

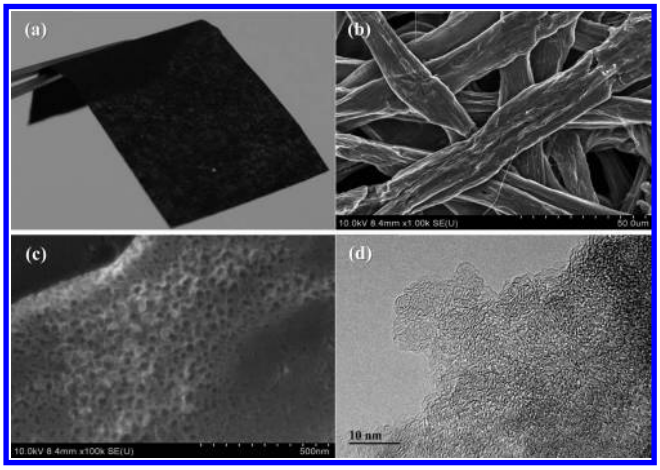


**Figure 2.** SEM and TEM images of CMWF derived from wood fiber electrode. (a) Photograph of CMWF. SEM images of CMWF to show the fiber morphology (b) and porous structure (c). (d) High-resolution TEM image of CMWF.

photograph of the free-standing and flexible carbon film derived from wood microfiber. The fiber morphology is well-maintained after carbonization as shown in Figure 2b. The percolated carbonized fibers ensure an efficient electron transfer along the fibers. When focused on the surface of each carbon fiber, numerous small pores in carbon fibers can be observed in Figures 2c and S2. The pores, which facilitate the diffusion of


DOI: 10.1021/acsami.7b01205
ACS Appl. Mater. Interfaces 2017, 9, 14801−14807

electrolyte in the CMWF, are inherited from wood microfibers, taking on a function as electrolyte reservoir. The high-resolution TEM image in Figure 2d suggests the obtained carbon is an amorphous carbon with visible secondary pores (>20 nm), which are too large to confine polysulfides and alleviate shuttle reaction.[46] It is pivotal to check if there are mesopores in CMWF and f-CMWF, which are invisible in SEM and TEM images. Thus, BET measurements are performed to confirm the existence of small size mesopores in f-CMWF.

As shown in Figures 3a and S3, the mesopores with sizes ranging from 3 to 12 nm exist in f-CMWF. The leftmost peaks

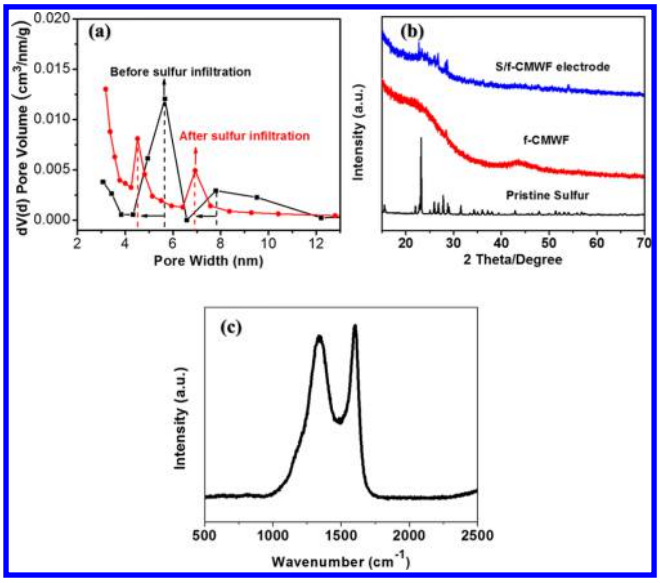


**Figure 3.** (a) BET dV(d) pore volume vs pore width distribution curve of the f-CMWF before and after sulfur infiltration. The black curve indicates the pore distribution before sulfur infiltration, and the red curve indicates the pore distribution after sulfur infiltration. The shift of the peaks indicates that the pores become smaller after sulfur infiltration. (b) XRD patterns for pristine sulfur, f-CMWF, and S/f-CMWF electrode; (c) Raman spectrum for f-CMWF.

at indicate even smaller pores (<3 nm) also exist in the fiber. The specific surface area and pore volume of f-CMWF are 586 $m^2\ g^{-1}$ and 0.27 $cm^3\ g^{-1}$, respectively. After sulfur infiltration, two peaks centered at the pore width of 5.7 and 7.8 nm shift to smaller values of 4.5 and 6.9 nm, respectively, demonstrating that the mesopores are filled with sulfur and the pore size becomes smaller. S/f-CMWF exhibits a specific surface area of 159 $m^2\ g^{-1}$ and a pore volume of 0.0798 $cm^3\ g^{-1}$. Therefore, SEM, TEM, and BET results confirm the porous structure of f-CMWF. The pores created for metabolism in trees are well-maintained after the fiber disintegration and carbonization process. The pores, especially the pores smaller than 5 nm, are able to confine sulfur in the conductive carbon matrix.

The content of sulfur in CMWF and f-CMWF is investigated by the thermogravimetric analysis (TGA). Demonstrated in Figure S4, both carbon films show very small weight loss of 4 and 8% in the temperature range from 80 to 800 °C, respectively, while the weight loss of carbon films with sulfur infiltration remarkably increases to 74 and 84% for S/f-CMWF electrode and S/CMWF electrode, respectively, demonstrating high sulfur loading of 70 and 76% in f-CMWF and CMWF. The high sulfur loading is due to the large pore volume of CMWF, which makes the current collector-free, binder and conductive additive-free electrodes very promising for LSB. The XRD patterns in Figures 3b and S5 show the XRD peaks for pristine sulfur, CMWF, f-CMWF electrode, S/CMWF, and S/f-CMWF electrode. No sharp peak can be observed in XRD patterns of CMWF and f-CMWF electrode, demonstrating amorphous structure of carbonized fiber before and after ALD, consistent with the result of high-resolution TEM in Figure 2d. After sulfur infiltration, the sharp peaks for sulfur can be observed in S/CMWF electrode, demonstrating successful sulfur infiltration in the mesoporous carbon, while the sulfur peaks in S/f-CMWF electrode are not as sharp as that in S/CMWF electrode. The Raman spectrum of f-CMWF in Figure 3c confirms the formation of conductive carbon after high-temperature carbonization of wood microfiber. The two sharps peaks at 1345 and 1595 $cm^{-1}$ represent $sp^3$-type disordered carbon and $sp^2$-type graphitic carbon, respectively with an intensity ratio close to 1.

The distribution of sulfur in the CMWF is characterized using SEM elemental mapping and high-resolution TEM (HRTEM). As shown in Figure S7a,b, most sulfur penetrated into the pores in the carbon fiber with a small quantity of sulfur coated on the S/CMWF electrode surface, while no sulfur can be observed in HRTEM image of the pure CMWF in Figure S8. The morphology of S/f-CMWF electrode is similar to that of CMWF as shown in Figure S6. SEM image (Figure S7c) and elemental mapping (Figures S7d and S9) of carbon, sulfur, and aluminum in the S/f-CMWF electrode show uniform distribution of Al and S in the S/f-CMWF electrode. No sulfur layer can be observed in HRTEM image of the S/f-CMWF electrode in Figure S10, demonstrating that most sulfur is encapsulated by mesopores in f-CMWF. As indicated by the SEM and TEM images of CMWF, the native pores are too large to confine sulfur, so extra sulfur is deposited on the surface of CMWF, while BET, elemental mapping, and HRTEM results indicate that the mesopores in f-CMWF are small enough to confine most sulfur. Therefore, S/f-CMWF electrode can be a promising cathode material for LSB.

The electrochemical performance of S/CMWF electrode and S/f-CMWF electrode is measured in coin cells. As shown in the cyclic voltammetry (CV) curves for S/CMWF electrode in Figure 4a, three cathodic peaks at 2.25, 2.05, and 1.35 V and two anodic peaks at 2.1 and 2.4 V are observed in the first scan. The peak at ~2.25 V corresponds to the lithiation of $S_8$ to soluble high-order polysulfides, confirming that $S_8$ on the surface is dissolved in the electrolyte during initial cycles; thus, severe shuttle reaction accompanied by fast capacity decay is displayed in S/CMWF electrode.[47−49] The peak at 2.05 V is attributed to the conversion of high-order polysulfide to low-order polysulfides, representing the redox reaction between S with Li during lithiation process in literatures.[49,50] The last peak at 1.35 V stands for the lithiation of small sulfur molecules ($S_{2-3}$), which can form insoluble lithium sulfides through the reaction with $Li^+$; thus, this peak is highly stable during the subsequent cycles. After the first scan, a shift of the peaks to the positive direction is observed due to the volume expansion of carbon matrix. To further characterize the electrochemical performance of sulfur in the carbon matrix, galvanostatic charge/discharge tests are carried out. Three lithiation plateaus at 2.35, 2.05, and 1.55 V, corresponding to three cathodic peaks in CV curves, can be observed in Figure 4b, while one slopping delithiation plateau centered at 2.1 V and one flat plateau at 2.4 V, corresponding to two anodic peaks in cyclic voltammogram, can also be observed.


DOI: 10.1021/acsami.7b01205
ACS Appl. Mater. Interfaces 2017, 9, 14801−14807

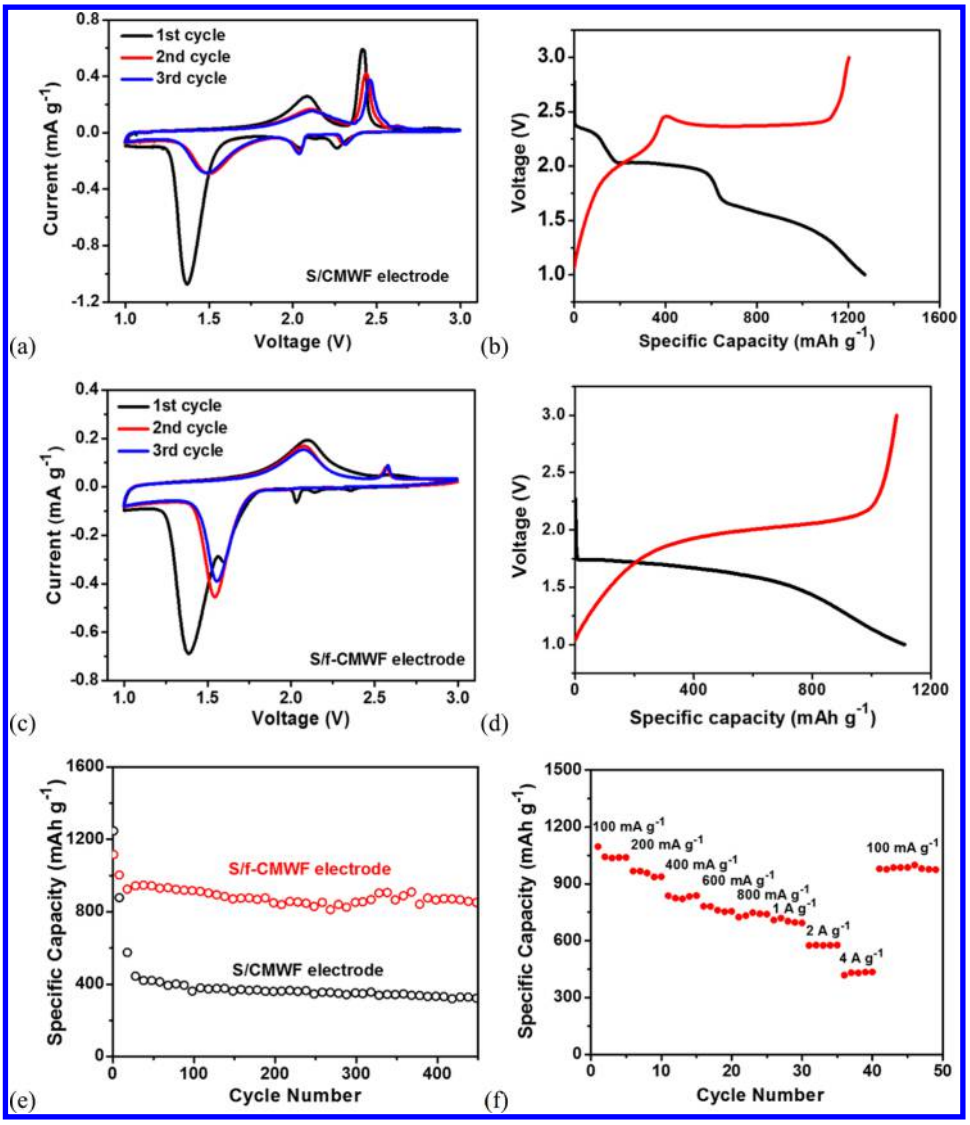


**Figure 4.** Electrochemical characterization of S/CMWF electrodes and S/f-CMWF electrodes. (a) CV performance for S/CMWF electrode at the first three cycles. (b) Galvanostatic charge/discharge performance of S/CMWF electrode. (c) CV for S/f-CMWF electrode at the first three cycles. (d) Galvanostatic charge/discharge performance of S/f-CMWF electrode. (e) Cycling stability test of S/CMWF electrodes and S/f-CMWF electrodes. (f) Specific capacity under different current density (rate performance) of the S/f-CMWF electrode.

For S/f-CMWF electrode, only large redox peaks at 1.55 and 2.1 V are observed after first cycle, attributed to the lithiation/delithiation of sulfur confined in mesopores as presented in the previous reports.[51,52] In Figure 4c, the redox peaks for high-order polysulfide ($Li_2S_8$) are very small and only observed in the first lithiation, while the redox peaks representing lithiation/delithiation of small sulfur molecules are much stronger than that in S/CMWF electrode, suggesting that S/f-CMWF electrode should have much better electrochemical performance. In galvanostatic charge/discharge curves (Figure 4d), there is only one pair of redox plateaus at 1.65 and 2.1 V for S/f-CMWF electrode, coincident with the CV curves in Figure 4c. No plateau for high-order polysulfides is observed, demonstrating that most sulfur is confined in the mesopores. During the initial cycles, the lithiation of the $Al_2O_3$ layer coated on the surface of carbonized wood fiber proceeds to form a thermodynamically stable phase composed of $Li_{3.4}Al_2O_3$ as reported by Han et al.[53] The interaction between small sulfur molecules and $Li_{3.4}Al_2O_3$ may also contribute to stabilize sulfur in the mesopores.

In the cycling test (Figure 4e), the S/CMWF electrode delivers an initial capacity of 1246 mAh $g^{-1}$ at 400 mA $g^{-1}$, while it suffers from fast capacity fading that the reversible capacity decreases to 442 mAh $g^{-1}$ in the 30th cycle. The fast initial capacity loss is caused by the dissolution of sulfur on CMWF surface. For comparison, S/f-CMWF cathode delivers a relatively lower initial capacity of 1115 mAh $g^{-1}$ at 400 mA $g^{-1}$ and maintains a reversible capacity of 859 mAh $g^{-1}$ for 450 cycles, corresponding to a very slow capacity decay rate of 0.046% per cycle. The better cycling stability for ALD-treated sample is ascribed to the thin layer of $Al_2O_3$, which reduces the pore size of CMWF to form more mesopores/micropores. The native pores of CMWF are too large to confine polysulfides, while the mesopores, formed after $Al_2O_3$ deposition, are ideal to confine polysulfides. The rate capability test (Figure 4f) is then carried out to check S/f-CMWF electrode under various current densities. At a low current density of 100 mA $g^{-1}$, S/f-CMWF delivers a high reversible capacity of 1000 mAh $g^{-1}$. When the current density increases to 4 A $g^{-1}$, the capacity can remain at 430 mAh $g^{-1}$. The excellent capacity retention is


DOI: 10.1021/acsami.7b01205
ACS Appl. Mater. Interfaces 2017, 9, 14801−14807

owed to the high conductivity and meso- and microporous structure of f-CMWF electrode, which facilitate the transport of lithium ion and electron in the electrode. After the current density is tuned back to 100 mA $g^{-1}$, the reversible capacity recovers immediately, demonstrating the superior robustness and integrity of the electrode.

## CONCLUSION

The f-CMWF electrode with unique hierarchical and mesoporous structure is first used as a host for sulfur cathode. Due to the high porosity of CMWF, 76 wt % sulfur can be infused into CMWF, which is a record high compared to the sulfur content in most reported work. $Al_2O_3$ deposition, which reduces the pore size of CMWF and slightly decreases the content (70 wt %) of sulfur in f-CMWF, remarkably enhances the cycling stability of sulfur cathode. The S/f-CMWF cathode delivers an initial capacity of 1115 mAh $g^{-1}$ at 400 mA $g^{-1}$ and maintains a reversible capacity of 859 mAh $g^{-1}$ for 450 cycles, corresponding to a very slow capacity decay rate of 0.046% per cycle. More importantly, the free-standing S/f-CMWF cathode is a current collector-free, binder and conductive additive-free electrode, which contains negligible electrochemical inactive component. The result in this work is not only important for fundamental study in LSB, but also important for using low cost and mesoporous biomass carbon as bifunctional scaffold for sulfur encapsulating.

## EXPERIMENTAL SECTION

**Fabrication of CMWF.** Natural wood fiber used in this work was from bleached pulp. Typically, 0.5 g of Kraft bleached softwood pulp was slushed into 100 mL of deionized water (DI water) and then mechanically stirred for 30 min at a speed of 1000 r $min^{-1}$. The pulp dispersion was then filtered by a vacuum filtration process through a membrane (diameter: 90 mm, pore-size: 0.65 $\mu$m, Millipore, U.S.A) and dried at 80 °C. Then, the wood fiber electrode was transferred into a tube furnace and stabilized at 240 °C for 8 h before being further carbonized at 1000 °C under argon for 2 h. The purpose of stabilizing bleached pulp at 240 °C for 8 h is to dewater the wood fiber, which can increase the yield of final product. From TGA (Figure S1), bleached pulp starts to be decomposed and carbonized at 300 °C, and it loses 90% of its initial weight at 800 °C.

**Atomic Layer Deposition Method.** ALD $Al_2O_3$ was carried out in a commercial BENEQ TFS 500 reactor (base pressure: 2 mbar). The process was done using trimethyl aluminum [TMA, $Al(CH_3)_3$] and DI water as precursors at 150 °C. The pulse time for TMA and DI water cycles were 250 ms. The thickness of the ALD $Al_2O_3$ deposited on Si wafer after 50 cycles was about 5 nm, as determined by a SOPRA GES5 spectroscopic ellipsometer.

**Sulfur Infiltration Process.** Sulfur and CMWF were mixed and sealed in a glass tube under vacuum with a weight ratio of 5:1. The sealed vacuum glass tube was first annealed in an oven at 600 °C for 5 h and then cooled to room temperature in 24 h. The resulting S/CMWF was collected and used as electrode for the battery test. A similar method is used to synthesize S/f-CMWF electrodes.

**Material Characterizations.** TGA (TA Instruments, USA) was carried out with a heating rate of 10 °C $min^{-1}$ in Ar gas; XRD pattern was obtained by Bruker Smart1000 (Bruker AXS Inc., USA) using Cu K$\alpha$ radiation. BET measurements were conducted using $N_2$ absorption on Micromeritics ASAP 2020 (Micromeritics Instrument Corp., USA).

**Electrochemical Measurements.** The free-standing S/CMWF is used as electrodes for LSB. The mass loading of the electrode is ~1.9 mg/$cm^2$, and sulfur mass loading is ~1.33 mg/$cm^2$. Coin cells were assembled with lithium metal as counter electrodes, 1.0 M bis(trifluoromethane) sulfonimide lithium salt (LiTFSI) in a mixture of dioxolane/dimethoxyethane (DOL/DME, 1:1 by volume) with 1% $LiNO_3$ as the electrolyte, and Celgard3501 (Celgard, LLC Corp., USA) as the separator. An Arbin battery test station (BT2000, Arbin Instruments, USA) was used to measure the electrochemical performance. Capacity was calculated based on the weight of sulfur. CV curves were recorded by Gamry Reference 3000 Potentiostat/Galvanostat/ZRA with a scan rate of 0.1 mV $s^{-1}$.

## ASSOCIATED CONTENT

### Supporting Information

The Supporting Information is available free of charge on the ACS Publications website at DOI: 10.1021/acsami.7b01205.

SEM images of CMWF; BET characterization of for CMWF and f-CMWF; thermogravimetric analysis for CMWF, f-CMWF, S/CMWF electrode and S/f-CMWF electrode; XRD patterns for CMWF and S/CMWF electrode; SEM image of S/f-CMWF electrode; high-resolution TEM image for CMWF; EDS mapping for S/CMWF electrode and S/f-CMWF electrode; high-resolution TEM image for S/f-CMWF electrode. (PDF)

## AUTHOR INFORMATION


### Corresponding Authors

*E-mail: cswang@umd.edu.
*E-mail: binghu@umd.edu.

### ORCID

Hongli Zhu: 0000-0003-1733-4333
Chunsheng Wang: 0000-0002-8626-6381
Liangbing Hu: 0000-0002-9456-9315


### Author Contributions

C.L. and H.Z. contributed equally to this work.

### Notes

The authors declare no competing financial interest.

## ACKNOWLEDGMENTS

This work was funded as part of the Nanostructures for Electrical Energy Storage (NEES), an Energy Frontier Research Center funded by the U.S. Department of Energy, Office of Science, Basic Energy Sciences, under Award number DESC0001160. We thank the support of Maryland Nano-Center and its AIMLab. The AIMLab is supported in part by the NSF as a MRSEC Shared Experimental Facility.

## REFERENCES


(1) Bruce, P. G.; Freunberger, S. A.; Hardwick, L. J.; Tarascon, J. M. Li-$O_2$ and Li-S Batteries with High Energy Storage. *Nat. Mater.* **2011**, *11*, 19−29.

(2) Yang, Y.; Zheng, G.; Cui, Y. Nanostructured Sulfur Cathodes. *Chem. Soc. Rev.* **2013**, *42*, 3018−3032.

(3) Manthiram, A.; Fu, Y.; Su, Y. S. Challenges and Prospects of Lithium-Sulfur Batteries. *Acc. Chem. Res.* **2013**, *46*, 1125−1134.

(4) Evers, S.; Nazar, L. F. New Approaches for High Energy Density Lithium-Sulfur Battery Cathodes. *Acc. Chem. Res.* **2013**, *46*, 1135−1143.

(5) Rosenman, A.; Markevich, E.; Salitra, G.; Aurbach, D.; Garsuch, A.; Chesneau, F. F. Review on Li-Sulfur Battery Systems: an Integral Perspective. *Adv. Energy Mater.* **2015**, *5*, 1500212.

(6) Yin, Y. X.; Xin, S.; Guo, Y. G.; Wan, L. J. Lithium−Sulfur Batteries: Electrochemistry, Materials, and Prospects. *Angew. Chem., Int. Ed.* **2013**, *52*, 13186−13200.

(7) Zhao, Y.; Wu, W.; Li, J.; Xu, Z.; Guan, L. Encapsulating MWNTs into Hollow Porous Carbon Nanotubes: A Tube-in-Tube Carbon Nanostructure for High-Performance Lithium-Sulfur Batteries. *Adv. Mater.* **2014**, *26*, 5113−5118.




DOI: 10.1021/acsami.7b01205
*ACS Appl. Mater. Interfaces* 2017, 9, 14801−14807

(8) Seh, Z. W.; Li, W.; Cha, J. J.; Zheng, G.; Yang, Y.; McDowell, M. T.; Hsu, P.-C.; Cui, Y. Sulphur-$TiO_2$ Yolk-Shell Nanoarchitecture with Internal Void Space for Long-Cycle Lithium-Sulphur Batteries. *Nat. Commun.* **2013**, *4*, 1331.
(9) Suo, L.; Hu, Y.-S.; Li, H.; Armand, M.; Chen, L. A New Class of Solvent-in-Salt Electrolyte for High-Energy Rechargeable Metallic Lithium Batteries. *Nat. Commun.* **2013**, *4*, 1481.
(10) Ji, X.; Evers, S.; Black, R.; Nazar, L. F. Stabilizing Lithium-Sulphur Cathodes Using Polysulphide Reservoirs. *Nat. Commun.* **2011**, *2*, 325.
(11) Deng, Y.; Xu, H.; Bai, Z.; Huang, B.; Su, J.; Chen, G. Durable Polydopamine-Coated Porous Sulfur Coreeshell Cathode for High Performance Lithium Sulfur Batteries. *J. Power Sources* **2015**, *300*, 386−394.
(12) Wang, J.; Yang, J.; Wan, C.; Du, K.; Xie, J.; Xu, N. Sulfur Composite Cathode Materials for Rechargeable Lithium Batteries. *Adv. Funct. Mater.* **2003**, *13*, 487−492.
(13) Yin, L.; Wang, J.; Lin, F.; Yang, J.; Nuli, Y. Polyacrylonitrile/Graphene Composite as a Precursor to A Sulfur-Based Cathode Material for High-Rate Rechargeable Li−S Batteries. *Energy Environ. Sci.* **2012**, *5*, 6966−6972.
(14) Zheng, S.; Han, P.; Han, Z.; Zhang, H.; Tang, Z.; Yang, J. High Performance C/S Composite Cathodes with Conventional Carbonate-Based Electrolytes in LSB. *Sci. Rep.* **2014**, *4*, 4842.
(15) Lu, L. Q.; Lu, L. J.; Wang, Y. Sulfur Film-Coated Reduced Graphene Oxide Composite for Lithium-Sulfur Batteries. *J. Mater. Chem. A* **2013**, *1*, 9173−9181.
(16) Zhang, S. S. Liquid Electrolyte Lithium/Sulfur Battery: Fundamental Chemistry, Problems, and Solutions. *J. Power Sources* **2013**, *231*, 153−162.
(17) Xin, S.; Gu, L.; Zhao, N.; Yin, Y.; Zhou, L.; Guo, Y.; Wan, L. Smaller Sulfur Molecules Promise Better Lithium-Sulfur Batteries. *J. Am. Chem. Soc.* **2012**, *134*, 18510−18513.
(18) Gao, J.; Lowe, M. A.; Kiya, Y.; Abruna, H. D. Effects of Liquid Electrolytes on the Charge-Discharge Performance of Rechargeable Lithium/Sulfur Batteries: Electrochemical and in-Situ X-ray Absorption Spectroscopic Studies. *J. Phys. Chem. C* **2011**, *115*, 25132−25137.
(19) Manthiram, A.; Fu, Y.; Chung, S.; Zu, C.; Su, Y. Rechargeable Lithium-Sulfur Batteries. *Chem. Rev.* **2014**, *114*, 11751−11787.
(20) Ji, X.; Lee, K. T.; Nazar, L. F. A Highly Ordered Nanostructured Carbon-Sulphur Cathode for Lithium−Sulphur Batteries. *Nat. Mater.* **2009**, *8*, 500−506.
(21) Wang, H.; Yang, Y.; Liang, Y.; Robinson, J. T.; Li, Y.; Jackson, A.; Cui, Y.; Dai, H. Graphene-Wrapped Sulfur Particles as a Rechargeable Lithium-Sulfur Battery Cathode Material with High Capacity and Cycling Stability. *Nano Lett.* **2011**, *11*, 2644−2647.
(22) Guo, J.; Xu, Y.; Wang, C. Sulfur-Impregnated Disordered Carbon Nanotubes Cathode for Lithium-Sulfur Batteries. *Nano Lett.* **2011**, *11*, 4288−4294.
(23) Ji, L.; Rao, M.; Zheng, H.; Zhang, L.; Li, Y.; Duan, W.; Guo, J.; Cairns, E. J.; Zhang, Y. Graphene Oxide as a Sulfur Immobilizer in High Performance Lithium/Sulfur Cells. *J. Am. Chem. Soc.* **2011**, *133*, 18522−18525.
(24) Ji, L.; Rao, M.; Aloni, S.; Wang, L.; Cairns, E. J.; Zhang, Y. Porous Carbon Nanofiber-Sulfur Composite Electrodes for Lithium/Sulfur Cells. *Energy Environ. Sci.* **2011**, *4*, 5053−5059.
(25) Jayaprakash, N.; Shen, J.; Moganty, S. S.; Corona, A.; Archer, L. A. Porous Hollow Carbon@Sulfur Composites for High-Power Lithium-Sulfur Batteries. *Angew. Chem., Int. Ed.* **2011**, *50*, 5904−5908.
(26) Elazari, R.; Salitra, G.; Garsuch, A.; Panchenko, A.; Aurbach, D. Sulfur-Impregnated Activated Carbon Fiber Cloth as a Binder-Free Cathode for Rechargeable Li-S Batteries. *Adv. Mater.* **2011**, *23*, 5641−5644.
(27) Schuster, J.; He, G.; Mandlmeier, B.; Yim, T.; Lee, K. T.; Bein, T.; Nazar, L. F. Spherical Ordered Mesoporous Carbon Nanoparticles with High Porosity for Lithium-Sulfur Batteries. *Angew. Chem., Int. Ed.* **2012**, *51*, 3591−3595.
(28) Guo, J.; Yang, Z.; Yu, Y.; Abruna, H. D.; Archer, L. A. Lithium-Sulfur Battery Cathode Enabled by Lithium-Nitrile Interaction. *J. Am. Chem. Soc.* **2013**, *135*, 763−767.
(29) Zhao, M. Q.; Zhang, Q.; Huang, J.-Q.; Tian, G.-L.; Nie, J.-Q.; Peng, H.-J.; Wei, F. Unstacked Double-Layer Templated Graphene for High-Rate Lithium-Sulphur Batteries. *Nat. Commun.* **2014**, *5*, 3410.
(30) Nan, C.; Lin, Z.; Liao, H.; Song, M. K.; Li, Y.; Cairns, E. J. Durable Carbon-Coated $Li_2S$ Core-Shell Spheres for High Performance Lithium/Sulfur Cells. *J. Am. Chem. Soc.* **2014**, *136*, 4659−4663.
(31) Xu, Y.; Wen, Y.; Zhu, Y.; Gaskell, K.; Cychosz, K. A.; Eichhorn, B.; Xu, K.; Wang, C. Confined Sulfur in Microporous Carbon Renders Superior Cycling Stability in Li/S Batteries. *Adv. Funct. Mater.* **2015**, *25*, 4312−4320.
(32) Chen, X.; Zhu, H.; Liu, C.; Chen, Y. C.; Weadock, N.; Rubloff, G.; Hu, L. Role of Mesoporosity in Cellulose Fibers for Electrode-Based Fast Electrochemical Energy Storage. *J. Mater. Chem. A* **2013**, *1*, 8201−8208.
(33) Hu, L.; Cui, Y. Energy and Environmental Nanotechnology in Conductive Electrode and Textiles. *Energy Environ. Sci.* **2012**, *5*, 6423−6435.
(34) Hu, L.; Wu, H.; La Mantia, F.; Yang, Y.; Cui, Y. Thin, Flexible Secondary Li-Ion Electrode Batteries. *ACS Nano* **2010**, *4*, 5843−5848.
(35) Gui, Z.; Zhu, H.; Gillette, E.; Han, X.; Rubloff, G. W.; Hu, L.; Lee, S. B. Natural Cellulose Fiber as Substrate for Supercapacitor. *ACS Nano* **2013**, *7*, 6037−6046.
(36) Zhu, H.; Jia, Z.; Chen, Y.; Weadock, N.; Wan, J.; Vaaland, O.; Han, X.; Li, T.; Hu, L. Tin Anode for Sodium-Ion Batteries Using Natural Wood Fiber as a Mechanical Buffer and Electrolyte Reservoir. *Nano Lett.* **2013**, *13*, 3093−3100.
(37) Zhu, H.; Fang, Z.; Preston, C.; Li, Y.; Hu, L. Transparent Electrode: Fabrications, Properties, and Device Applications. *Energy Environ. Sci.* **2014**, *7*, 269−287.
(38) Zhu, H.; Wang, H.; Li, Y.; Bao, W.; Fang, Z.; Preston, C.; Vaaland, O.; Ren, Z.; Hu, L. Lightweight, Conductive Hollow Fibers from Nature as Sustainable Electrode Materials for Microbial Energy Harvesting. *Nano Energy* **2014**, *10*, 268−276.
(39) Zheng, G.; Cui, Y.; Karabulut, E.; Wågberg, L.; Zhu, H.; Hu, L. Nanostructured Electrode for Flexible Energy and Electronic Devices. *MRS Bull.* **2013**, *38*, 320−325.
(40) Luo, C.; Zhu, Y.; Wen, Y.; Wang, J.; Wang, C. Carbonized Polyacrylonitrile-Stabilized $SeS_x$ Cathodes for Long Cycle Life and High Power Density Lithium Ion Batteries. *Adv. Funct. Mater.* **2014**, *24*, 4082−4089.
(41) Luo, C.; Xu, Y.; Zhu, Y.; Liu, Y.; Zheng, S.; Liu, Y.; Langrock, A.; Wang, C. Selenium@Mesoporous Carbon Composite with Superior Lithium and Sodium Storage Capacity. *ACS Nano* **2013**, *7*, 8003−8010.
(42) He, G.; Evers, S.; Liang, X.; Cuisinier, M.; Garsuch, A.; Nazar, L. F. Tailoring Porosity in Carbon Nanospheres for Lithium-Sulfur Battery Cathodes. *ACS Nano* **2013**, *7*, 10920−10930.
(43) Ye, X.; Ma, J.; Hu, Y.; Wei, H.; Ye, F. MWCNT Porous Microspheres with an Efficient 3D Conductive Network for High Performance Lithium-Sulfur Batteries. *J. Mater. Chem. A* **2016**, *4*, 775−780.
(44) Jin, F.; Xiao, S.; Lu, L.; Wang, Y. Efficient Activation of High-Loading Sulfur by Small CNTs Confined Inside a Large CNT for High-Capacity and High-Rate Lithium-Sulfur Batteries. *Nano Lett.* **2016**, *16*, 440−447.
(45) Fang, X.; Weng, W.; Ren, J.; Peng, H. A Cable-Shaped Lithium Sulfur Battery. *Adv. Mater.* **2016**, *28*, 491−496.
(46) Zhang, B.; Qin, X.; Li, G. R.; Gao, X. P. Enhancement of Long Stability of Sulfur Cathode by Encapsulating Sulfur into Micropores of Carbon Spheres. *Energy Environ. Sci.* **2010**, *3*, 1531−1537.
(47) Wu, F.; Ye, Y.; Chen, R.; Qian, J.; Zhao, T.; Li, L.; Li, W. Systematic Effect for an Ultralong Cycle Lithium-Sulfur Battery. *Nano Lett.* **2015**, *15*, 7431−7439.
(48) Oschmann, B.; Park, J.; Kim, C.; Char, K.; Sung, Y.-E.; Zentel, R. Copolymerization of Polythiophene and Sulfur to Improve the


DOI: 10.1021/acsami.7b01205
*ACS Appl. Mater. Interfaces* 2017, 9, 14801−14807

Electrochemical Performance in Lithium-Sulfur Batteries. *Chem. Mater.* **2015**, *27*, 7011−7017.
(49) Li, G.; Ling, M.; Ye, Y.; Li, Z.; Guo, J.; Yao, Y.; Zhu, J.; Lin, Z.; Zhang, S. Acacia Senegal-Inspired Bifunctional Binder for Longevity of Lithium-Sulfur Batteries. *Adv. Energy Mater.* **2015**, *5*, 1500878.
(50) Zheng, S.; Wen, Y.; Zhu, Y.; Han, Z.; Wang, J.; Yang, J.; Wang, C. In Situ Sulfur Reduction and Intercalation of Graphite Oxides for Li-S Battery Cathodes. *Adv. Energy Mater.* **2014**, *4*, 1400482.
(51) Zheng, S.; Yi, F.; Li, Z.; Zhu, Y.; Xu, Y.; Luo, C.; Yang, J.; Wang, C. Copper-Stabilized Sulfur-Microporous Carbon Cathodes for Li-S Batteries. *Adv. Funct. Mater.* **2014**, *24*, 4156−4163.
(52) Luo, C.; Zhu, Y.; Borodin, O.; Gao, T.; Fan, X.; Xu, Y.; Xu, K.; Wang, C. Activation of Oxygen-Stabilized Sulfur for Li and Na Batteries. *Adv. Funct. Mater.* **2016**, *26*, 745−752.
(53) Jung, S. C.; Han, Y. K. How Do Li Atoms Pass through the $Al_2O_3$ Coating Layer during Lithiation in Li-ion Batteries? *J. Phys. Chem. Lett.* **2013**, *4*, 2681−2685.


DOI: 10.1021/acsami.7b01205
*ACS Appl. Mater. Interfaces* 2017, 9, 14801−14807